J6.12   TURBULENT FLOW OVER ISOLATED RIDGES;
INFLUENCE OF VEGETATION

Edward G. Patton[1,*], Peter P. Sullivan[1] and Keith Ayotte[2]

[1]National Center for Atmospheric Research, Boulder, CO
[2]Windlab Systems, Canberra, ACT, Australia

1. INTRODUCTION

Characterizing the turbulence associated with flow over forested hills is of distinct interest for wind energy applications Ayotte and Hughes (2004). In particular, studies of turbulent flow associated with canopy-covered hills will help turbine manufacturers design machines capable of operating in complex environments. In addition, studies of this kind will help in the positioning of wind farms since further quantification of turbulent characteristics over canopy-covered hills will provide more confidence to wind resource developers as they search for ideal locations to harness wind power.

It is also widely recognized that when used over forested hills, the aerodynamic (eddy covariance) method of measuring surface exchange fails to accurately capture night-time fluxes under stably stratified atmospheric conditions (Baldocchi, 2003). A prime suspect for this discrepancy is drainage flows away from towers (Staebler, 2003), which in complex terrain are predominantly located on high ground.

Recent studies using analytic models (*e.g.,* Finnigan and Belcher, 2004; Ross and Vosper, 2005) show distinct differences between turbulent flows over sinusoidal hills with specified roughness and those with tall, porous vegetation. In particular, they show that: 1) with resolved vegetation, above-canopy velocities are greatest on the windward side of the hill, 2) overall speed-up above the canopy at the crest of the hill is diminished compared to hills with specified roughness, and 3) that due to this upstream shift, within-canopy velocities on the leeward side of the hill recirculate on hills that would otherwise not separate. These findings have important implications for both measurement interpretation and wind energy deployment in undulating terrain. Here, we use our LES to investigate these findings for isolated hills.

---
corresponding author address: Edward G. Patton, National Center for Atmospheric Research, P. O. Box 3000, Boulder, CO 80307-3000; *email*: patton@ucar.edu

Figure 1: Photo of the wind tunnel configuration in Ayotte and Hughes (2004). Here the hill shape is being measured. Sand covers the hill serving as roughness.

2. NUMERICAL METHODS

We have extend our canopy-resolving large-eddy simulation (LES) code, which has demonstrated high skill in simulating three-dimensional canopy-resolving turbulent flows in neutral and convective conditions (Patton, 1997; Dwyer et al., 1997; Patton et al., 2003) and even with chemical reaction Patton et al. (2001), to modestly complex terrain. The LES code has recently been adapted to a curvilinear coordinate system (Sullivan et al., 2000, 2004) allowing investigation of two-dimensional hilly terrain.

For the with-canopy cases, we include a term in the Navier-Stokes equations representing the drag imposed by the forest canopy which is written as

$$F_i = -C_d a \mathrm{U} u_i \,. \qquad (1)$$

Where, C_d is an isotropic drag coefficient, a is leaf area density (one-sided leaf area per unit volume), and U represents the current wind speed, $(u_i u_i)^{\frac{1}{2}}$, and u_i is the resolved velocity in the i-direction.

3. SIMULATIONS

In general, we model our cases after measurements reported in Ayotte and Hughes (2004) (see Figure 1). Four simulations are compared and contrasted. Each of these cases use $800 \times 200 \times 144$ grid points representing a $4 \times 1 \times 1.8$ km^3 domain. The runs are driven by a specified large-scale normalized pressure gradient ($\frac{1}{\rho} \frac{\partial P}{\partial x}$) in the x-direction of 1.225×10^{-4} ms^{-2}. Buoyancy forces are neglected such that we are considering only neutral stratification. Lateral boundary conditions are periodic and the upper boundary is a a frictionless rigid lid. The lower boundary condition defines the four cases that we will consider.

The first case mimics the 0.2S case presented by Ayotte and Hughes (2004). The bottom surface is of specified roughness ($z_o = 0.075$ m) which comes directly from scaling the z_o estimated from the undisturbed velocity profile measured in the wind tunnel. The lower surface is is defined by a two-dimensional isolated hill (*i.e.,* there is no terrain variation in the lateral (y) direction) with the following specified shape:

$$
\begin{aligned}
z &= a\left(1 + \cos\left(\tfrac{\pi}{2}\tfrac{x}{L}\right)\right) & -2L \geq x \geq 2L \\
z &= 0 & \text{otherwise}
\end{aligned} \tag{2}
$$

where, the hill half-length $L = 250$ m, and the amplitude $a = 31.831$ which is chosen to give a maximum hill slope of 0.2. This occurs at the midpoint of the windward/leeward hill faces. The ratio of the hill height to half-length (H/L) is 0.25; H is 62.5 m. To ensure that the hill remains isolated we extend our horizontal domain to $16L$ to allow ample time and distance for the flow to recover before the flow encounters the hill again because of the periodic boundary conditions.

Three more cases are considered. The first is flat but throughout the lowest twenty meters of the domain (10 vertical grid points over all x and y) we distribute canopy elements of equal density. The canopy's plant area index is about 10.6. We use this case to determine the effective z_o of the canopy in a horizontally homogeneous regime. The last two cases are identical to the first in that the bottom surface of both is described by Equation 2, although one uses a specified surface roughness (the effective z_o found for the canopy in the flat case) which we'll call the *roughness* case, and the other contains the vertically distributed canopy which we'll call the *canopy* case. Due to the curvilinear coordinate system, the canopy is resolved by eight grid points in the flat region of the domain, increasing to 14 grid points at the top of the hill.

Due to the high cost of these neutrally-buoyant simulations, the simulations were initiated using coarse resolution ($200 \times 50 \times 144$ grid points) and were run out to equilibrium, about 60,000 time steps. The 3D fields were then stored, spectrally interpolated to the fine resolution, and then the simulations were restarted. Integration continued at this high-resolution for another 20,000 steps, or about fifty minutes of simulated time. The results presented are averaged over the last 10,000 steps (approximately thirty minutes) after the energy spectrum filled out completely and the flow reached equilibrium again.

4. RESULTS

4.1 Comparison with measurements

To validate the LES results over an isolated ridge, we compare our simulations with the wind tunnel measurements reported in Ayotte and Hughes (2004). Laterally- and time-averaged streamwise velocity profiles agree extremely well with the measurements shown in Figure 2, however they deviate some from the measurements on the lee side of the hill. Neither the flow in the tunnel or that in the LES separate on average. Although great efforts were made to minimize potential pressure reflections from the upper wall in the tunnel, it is possible that the tunnel flow is being squeezed by that upper boundary. As such, the flow in the tunnel is possibly being forced back down the lee side of the hill, thereby revealing stronger velocities than the LES in this region since it is not so constricted. In addition, due to the lengthy integration times, the boundary layer in the LES has cycled through the domain many times, while the boundary layer in the tunnel was tripped only $65L$ upstream of the hill.

Lateral- and time-averaged vertical turbulent momentum fluxes also compare reasonably well with the tunnel measurements upstream of the hill (Figure 3). In the lee of the hill, the LES-derived momentum fluxes increase compared to the tunnel in a manner which is consistent with the LES's increased velocity shear shown in Figure 2.

These comparisons show that both mean and first-order turbulent quantities are well reproduced by the LES for flows over isolated hills with specified z_o. We now examine the relationship between isolated hills of specified roughness and those with resolved tall vegetation.

4.2 Resolved vegetation vs. specified roughness

Compared to velocity profiles at $x/L = 0$, cases with specified roughness and resolved vegetation both show little modification to lateral- and time-averaged streamwise velocities at the base of the hill ($x/L = -2$, see Figure 4). Consistent with the theory for low hills by Finnigan and Belcher (2004), the flow above the canopy speeds up on the windward side of the hill ($x/L = -1$) compared to the case with specified roughness length. At the hill crest
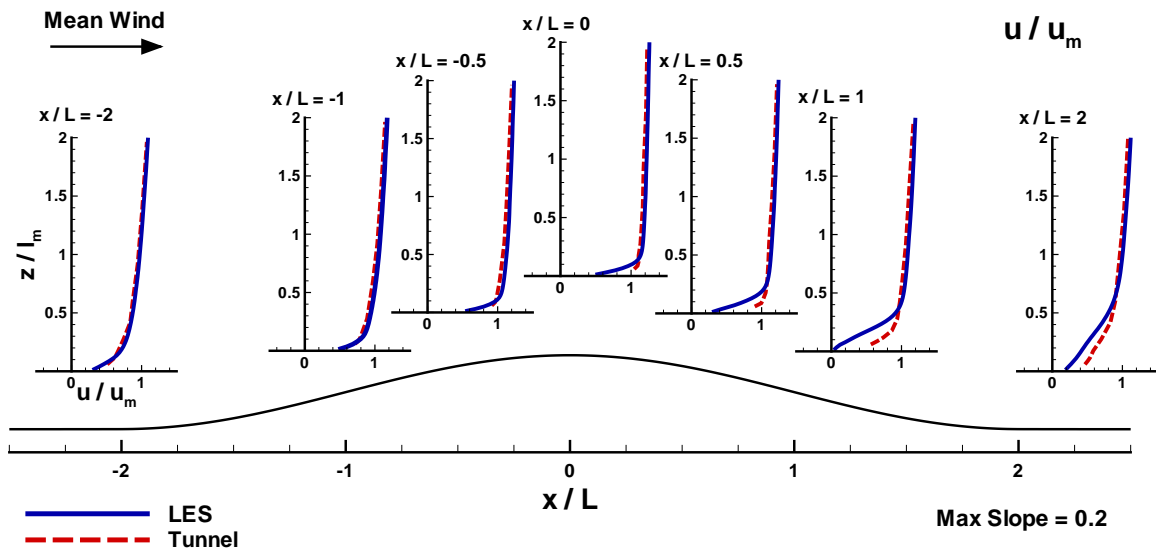
Figure 2: A comparison of laterally- and time-averaged profiles of streamwise velocity at x/L = [-2, -1, -0.5, 0, 0.5, 1, and 2] from LES and wind tunnel measurements. The mean wind is from left to right. Variables are normalized by the height of the middle-layer depth (l_m, see Hunt et al. 1988 for details) and the velocity at that depth from the undisturbed velocity profile well upwind of the hill (u_m).
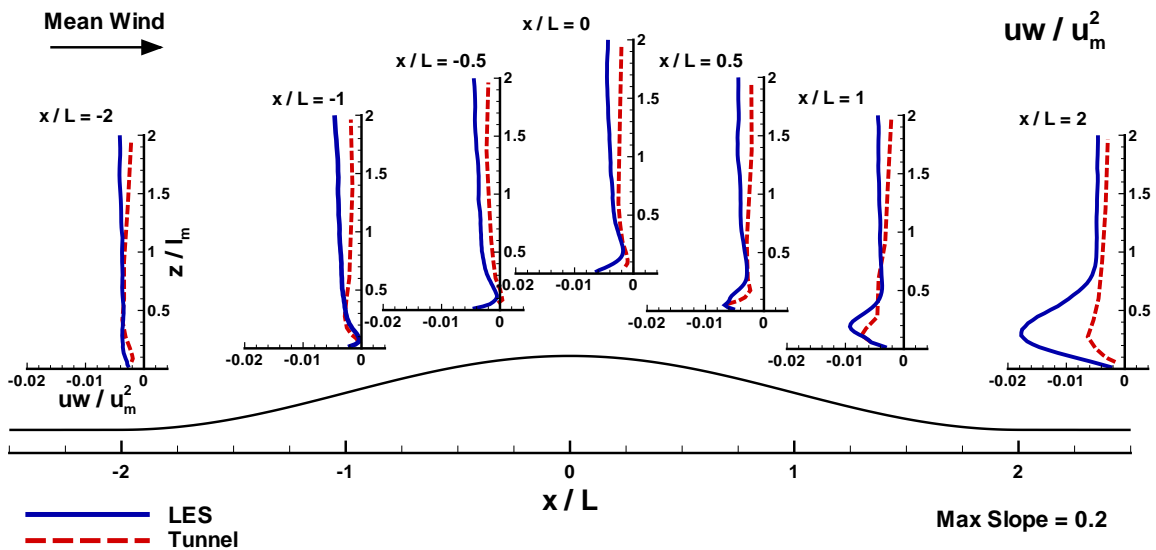

Figure 3: A comparison of laterally- and time-averaged profiles of vertical momentum flux at x/L = [-2, -1, -0.5, 0, 0.5, 1, and 2] from LES and wind tunnel measurements. The mean wind is from left to right. Variables are normalized by the height of the middle-layer depth (l_m, see Hunt et al. 1988 for details) and the velocity at that depth from the undisturbed velocity profile well upwind of the hill (u_m). The LES fluxes include both the resolved and sub-filter scale components.
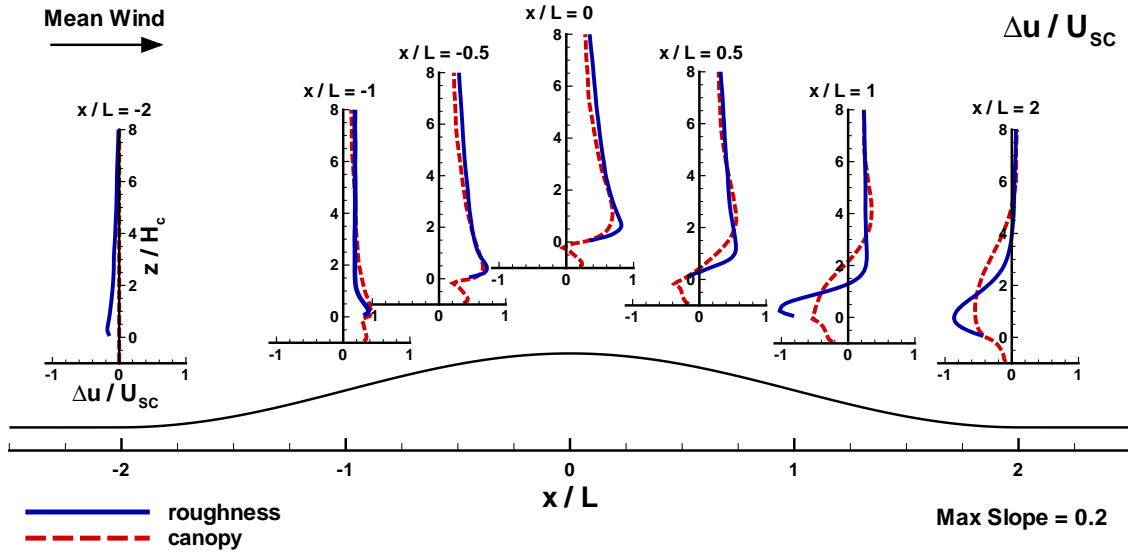
Figure 4: Profiles comparing the relative speed up compared to the upwind-most profile of laterally- and time-averaged streamwise velocity, *i.e.*, $\Delta u(x/L, z/H_c) = u(x/L, z/H_c) - u(-8, z/H_c)$, at locations $x/L = [-2, -1, -0.5, 0, 0.5, 1,$ and $2]$ from the *roughness* and *canopy* cases. The mean wind is from left to right. The vertical coordinate is normalized by the canopy height (H_c) and the reference has been shifted such that the top of the vegetation now refers to z/H_c=0. Velocity is normalized by the vertically integrated streamwise velocity at x/L=-8, U_{SC}.

and above the vegetation, the *canopy* case is slightly retarded compared to the *roughness* case. Both cases show a dramatic wind speed reduction on the hill's leeward side, but consistent with theory (Finnigan and Belcher, 2004) the within-canopy flow for the *canopy* case is on average negative in sign, although only weakly recirculating (not shown). This separation results because of the increased canopy drag near the surface. In the momentum equations valid for canopy flow, momentum flux divergence serves to bring momentum to regions of deficit, while drag acts as a momentum sink. Therefore in the lee of the hill it appears that with the canopy-imposed drag, the momentum flux divergence is unable to counter the pressure gradient induced by the hill resulting in recirculating flow. As shown in Figure 2, recirculation in the lee of the hill is not present in the *roughness* case.

To elucidate this further, Figure 5 shows the horizontal variation of normalized surface pressure ($p/\rho U_{SC}^2$) from the two cases. Although the pressure gradients are not as large in the *canopy* case, it exhibits greater asymmetry of the pressure field and thus larger total drag. Belcher et al. (1993) showed that pressure drag induced by the hill, *i.e.,* a downwind shift or asymmetry of the hill-induced pressure minimum which results in a net windward force on the hill, is the leading order term in extracting momentum from turbulent flow over hills with specified roughness. As suggested by Finnigan and Belcher (2004) and

Ross and Vosper (2005) for sinusoidal hills, our results confirm that pressure drag associated with tall canopies also increases the total drag for isolated hills. It is therefore worth noting that large-scale models attempting to parameterize unresolved orography of this sort will need to modify the parameterization to include vegetation effects.

For both wind energy applications and scalar transport, it is prudent to establish the relative importance of the aforementioned wind speed accelerations/decelerations on the turbulence. Therefore, we present the relative turbulence intensities in Figure 6. At almost all heights and horizontal locations, the fluctuations in the *canopy* case are larger than those in the case with specified *roughness*. Before the hill, wind speeds in the canopy case are small near the ground compared to the streamwise velocity fluctuations. On the windward side of the hill, velocity fluctuations in both cases remain at a similar relationship with respect to the local scalar wind speed (U). For the *roughness* case, at the crest where the speed-up over the hill is the greatest, turbulence intensities diminish somewhat compared to the windward side of the hill. The same is true for the *canopy* case above z/H_c=2, but below this height (within the roughness sublayer), turbulence intensities begin to increase. This increase largely results from a reduction in the mean wind as the pressure gradient over the hill
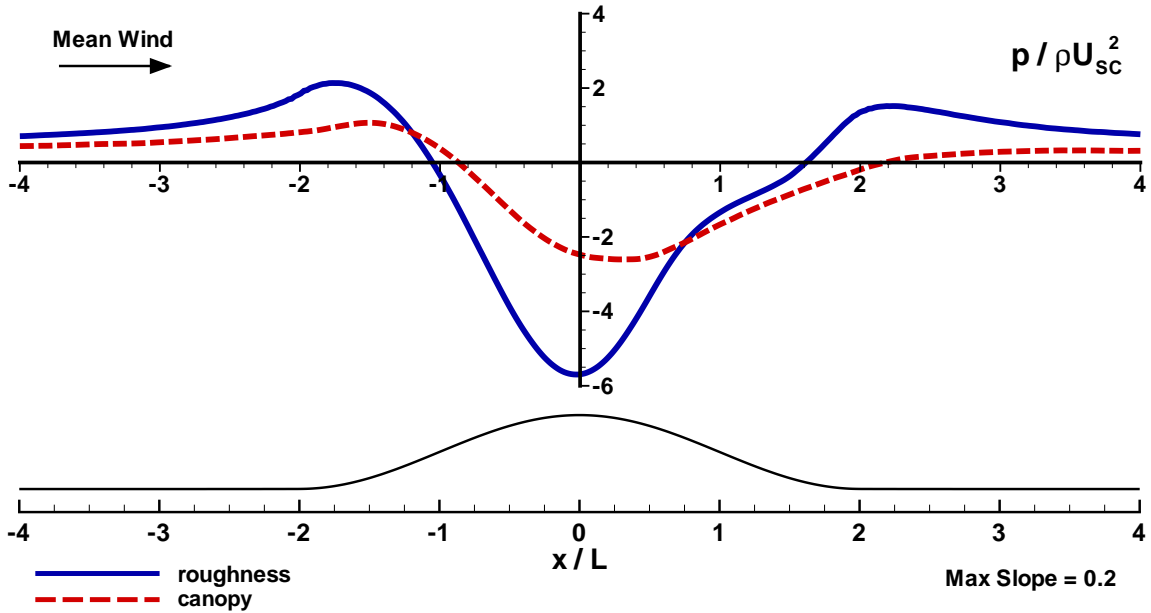
Figure 5: Horizontal profiles of the lateral- and time-averaged surface pressure (p/ρ) normalized by U_{SC}^2 from the *roughness* and *canopy* cases. The mean wind is from left to right.
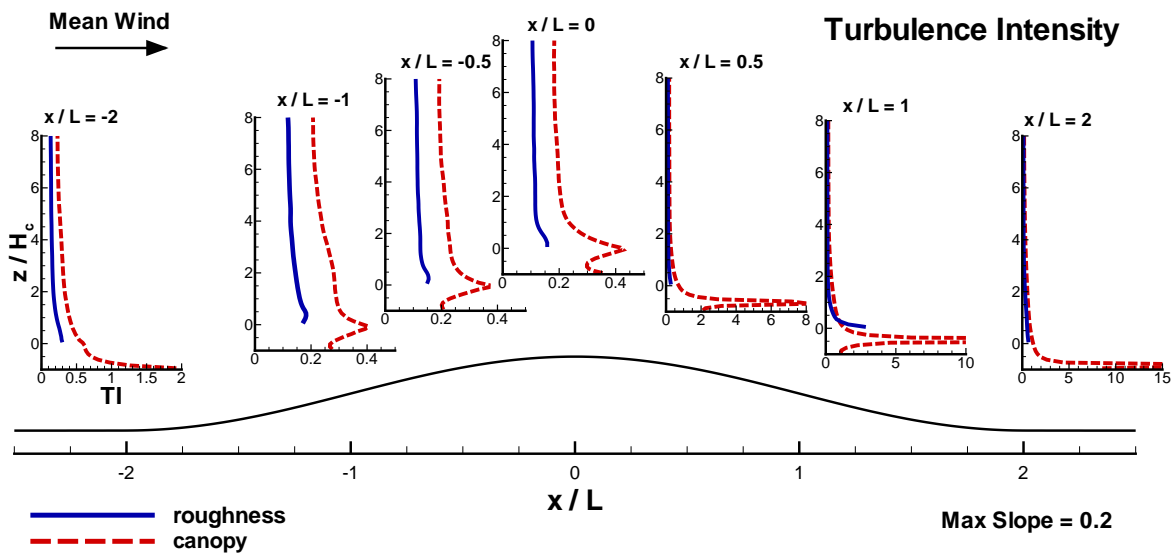

Figure 6: Vertical profiles comparing laterally- and time-averaged turbulence intensity (σ_u/U)) at locations $x/L = [-2, -1, -0.5, 0, 0.5, 1,$ and $2]$ from the *roughness* and *canopy* cases. The mean wind is from left to right. The vertical coordinate is normalized by the canopy height (H_c) and has been shifted such that the top of the vegetation now refers to $z/H_c=0$. Here, $|U|$) refers to the local lateral- and time averaged cup wind speed. Note that the range of the abscissa changes for each x/L.

begins to relax (see Figure 5) and the pressure drag from the canopy becomes more important. Aloft in the hill's lee, the velocity perturbations are comparable between the two cases, although somewhat larger in the canopy case. While at the canopy top, the mean winds become extremely small, increasing the turbulence intensities at this height. Deep within the canopy, the turbulence is strong yet the mean winds can't overcome the adverse pressure gradient and return up the hill, which can be seen by the somewhat diminished intensities deep within the vegetation.

5. IMPACTS AND CONCLUSIONS

Mean and first-order turbulence statistics from LES of flow over isolated hills of specified roughness compares well with wind tunnel measurements. Turbulent flow over tall vegetation on isolated hills is shown to have similar impact as flow over canopy-covered sinusoidal hills. Flows with resolved vegetation are shown to exhibit nearly twice the turbulence intensity of that found in cases with specified roughness.

These results suggest that when deploying wind turbines at the crest of forested hills, wind turbines will need to be able to handle this increased turbulence intensity. They should also expect only a slight reduction in productive capacity compared to hills without tall vegetation given the minimal speed-up reduction over the hill compared to hills with short vegetation. With the propensity for tall vegetation to grow in the presence of orography, the added cost embedded in building sturdier turbines will certainly be offset by the ability to expand what would be considered a deployable regime.

With respect to tower observations in the vicinity of isolated hills, our results suggest that these measurements need to be interpreted cautiously. Scalar transport could easily be occurring which would not be detectable by an instrument located on a tower above the trees.

REFERENCES

Ayotte, K. W. and D. E. Hughes, 2004: Observations of boundary-layer wind-tunnel flow over isolated ridges of varying steepness and roughness, *Boundary-Layer Meteorol.*, **112**, 525–556.

Baldocchi, D. D., 2003: Assessing the eddy covariance technique for evaluating carbon dioxide exchange rates of ecosystems: past, present and future, *Glob. Change Biol.*, **9**, 479–492.

Belcher, S. E., T. M. Newley, and J. C. R. Hunt, 1993: The drag on an undulating surface induced by the turbulent boundary layer, *J. Fluid Mech.*, **249**, 557–596.

Dwyer, M. J., E. G. Patton, and R. H. Shaw, 1997: Turbulent kinetic energy budgets from a large-eddy simulation of flow above and within a forest canopy, *Boundary-Layer Meteorol.*, **84**, 23–43.

Finnigan, J. J. and S. E. Belcher, 2004: Flow over a hill covered with a plant canopy, *Quart. J. Roy. Meteorol. Soc.*, **130**, 1–29.

Hunt, J. C. R., S. Leibovich, and K. J. Richards, 1988: Turbulent shear flows over low hills, *Quart. J. Roy. Meteorol. Soc.*, **114**, 1435–1471.

Patton, E. G., 1997: *Large-eddy simulation of turbulent flow above and within a plant canopy*, Ph.D. thesis, University of California, Davis, California.

Patton, E. G., K. J. Davis, M. C. Barth, and P. P. Sullivan, 2001: Decaying scalars emitted by a forest canopy: A numerical study, *Boundary-Layer Meteorol.*, **100**, 91–129.

Patton, E. G., P. P. Sullivan, and K. J. Davis, 2003: The influence of a forest canopy on top-down and bottom-up diffusion in the planetary boundary layer, *Quart. J. Roy. Meteorol. Soc.*, **129**, 1415–1434.

Ross, A. N. and S. B. Vosper, 2005: Neutral turbulent flow over forested hills, *Quart. J. Roy. Meteorol. Soc.*, **131**, 1841–1862.

Staebler, R. M., 2003: *Forest subcanopy flows and micro-scale advection of carbon dioxide*, Ph.D. thesis, State University of New York, Albany, New York.

Sullivan, P. P., J. B. Edson, J. C. McWilliams, and C.-H. Moeng, 2004: Large-eddy simulations and observations of wave-driven boundary layers, in *16th Amer. Meteorol. Soc. Symp. on Boundary Layers and Turb.*, Portland, ME, http://ams.confex.com/ams/pdfpapers/78119.pdf.

Sullivan, P. P., J. C. McWilliams, and C.-H. Moeng, 2000: Simulation of turbulent flow over idealized water waves, *J. Fluid Mech.*, **404**, 47–85.